Evidence for the two-body charmless baryonic decay $ {B}^{+}\to p\overline{\varLambda} $

Evidence for the two-body charmless baryonic decay $B^+ \to p\bar{\Lambda}$

The LHCb collaboration

E-mail: eduardo.rodrigues@cern.ch

ABSTRACT: A search for the rare two-body charmless baryonic decay $B^+ \to p\bar{\Lambda}$ is performed with pp collision data, corresponding to an integrated luminosity of 3 fb^{-1}, collected by the LHCb experiment at centre-of-mass energies of 7 and 8 TeV. An excess of $B^+ \to p\bar{\Lambda}$ candidates with respect to background expectations is seen with a statistical significance of 4.1 standard deviations, and constitutes the first evidence for this decay. The branching fraction, measured using the $B^+ \to K_S^0 \pi^+$ decay for normalisation, is

$$\mathcal{B}(B^+ \to p\bar{\Lambda}) = (2.4\,^{+1.0}_{-0.8} \pm 0.3) \times 10^{-7},$$

where the first uncertainty is statistical and the second systematic.

Contents

1 Introduction

The experimental study of B meson decays to baryonic final states has a long history, including numerous searches and observations by the asymmetric e^+e^- collider experiments BaBar and Belle [1]. In recent years the LHCb collaboration reported the first observation of a two-body charmless baryonic B^+ decay and the first evidence for a similar B^0 decay, namely $B^+ \to p\overline{\Lambda}(1520)$ [2] and $B^0 \to p\overline{p}$ [3]. No other two-body charmless baryonic B decay modes have been observed. Their experimental study requires large data samples, presently only available at the LHC, as baryonic B decays to two-body final states are suppressed, with branching fractions typically one to two orders of magnitude lower than similar baryonic decays to multibody final states.

Experimental input on the branching fractions of the $B^+ \to p\overline{\Lambda}$ decay and other suppressed baryonic decays provides valuable information on the dynamics of the decays of B mesons to baryonic final states. The $B^+ \to p\overline{\Lambda}$ decay mode is expected to be dominated by a $b \to s$ loop transition, but tree-level (V_{ub} suppressed) and annihilation diagrams also contribute. Various theoretical predictions for its branching fraction are available. Calculations based on QCD sum rules [4] predict a branching fraction smaller than 3×10^{-6} whereas a pole model [5] and a recent study [6], taking into account the LHCb experimental result on the $B^0 \to p\overline{p}$ branching fraction [3], both predict a branching fraction around 2×10^{-7}. The violation of partial conservation of the axial-vector current at the GeV scale has been proposed as an alternative approach to the understanding of the data available on two-body baryonic decays of B and D_s^+ mesons [7]. It explains the LHCb results on the $B_{(s)}^0 \to p\overline{p}$ decay modes [3] and predicts a branching fraction for the $B^+ \to p\overline{\Lambda}$ decay of the order of 10^{-8}.

The decay $B^+ \to p\overline{\Lambda}$ has been searched for by the CLEO [8] and Belle [9] collaborations. The most stringent experimental upper limit on the $B^+ \to p\overline{\Lambda}$ branching fraction is 3.2×10^{-7} at 90% confidence level, determined by the Belle collaboration using $414\,\text{fb}^{-1}$ of integrated luminosity from e^+e^- collisions.

This paper presents a search for the rare decay mode $B^+ \to p\overline{\Lambda}$ with the full pp collision data sample collected in 2011 and 2012 by the LHCb experiment. The branching fraction is measured with respect to that of the topologically identical $B^+ \to K_S^0 \pi^+$ decay to suppress common systematic uncertainties. The Λ baryon is reconstructed in the $\Lambda \to p\pi^-$ final state whereas the K_S^0 meson is reconstructed in its $K_S^0 \to \pi^+\pi^-$ final state. The inclusion of charge-conjugate processes is implied throughout this paper.

2 Detector and data sample

The data sample analysed corresponds to an integrated luminosity of $1\,\text{fb}^{-1}$ at a centre-of-mass energy of 7 TeV recorded in 2011 and $2\,\text{fb}^{-1}$ at 8 TeV recorded in 2012. The LHCb detector [10, 11] is a single-arm forward spectrometer covering the pseudorapidity range $2 < \eta < 5$, designed for the study of particles containing b or c quarks. The detector includes a high-precision tracking system consisting of a silicon-strip vertex detector surrounding the pp interaction region, a large-area silicon-strip detector located upstream of a dipole magnet with a bending power of about $4\,\text{Tm}$, and three stations of silicon-strip detectors and straw drift tubes placed downstream of the magnet. The tracking system provides a measurement of momentum, p, of charged particles with a relative uncertainty that varies from 0.5% at low momentum to 1.0% at $200\,\text{GeV}/c$. The minimum distance of a track to a primary vertex (PV), the impact parameter (IP), is measured with a resolution of $(15 + 29/p_\text{T})\,\mu\text{m}$, where p_T is the component of the momentum transverse to the beam, in GeV/c. The different types of charged hadrons are distinguished using information from two ring-imaging Cherenkov detectors. Photons, electrons and hadrons are identified by a calorimeter system consisting of scintillating-pad and preshower detectors, an electromagnetic calorimeter and a hadronic calorimeter. Muons are identified by a system composed of alternating layers of iron and multiwire proportional chambers.

The decays of the V^0 hadrons, namely $\Lambda \to p\pi^-$ and $K_S^0 \to \pi^+\pi^-$, are reconstructed in two different categories: the first consists of V^0 hadrons that decay early enough for the daughter particles to be reconstructed in the vertex detector, and the second contains those that decay later such that track segments cannot be reconstructed in the vertex detector. These categories are referred to as *long* and *downstream*, respectively. The candidates in the long category have better mass, momentum and vertex resolution than those in the downstream category.

Events are selected in a similar way for both the $B^+ \to p\overline{\Lambda}$ signal decay and the normalisation channel $B^+ \to K_S^0 \pi^+$. The online event selection is performed by a trigger consisting of a hardware stage, based on information from the calorimeter and muon systems, followed by a software stage that performs a full event reconstruction, in which all charged particles with $p_\text{T} > 500\,(300)\,\text{MeV}/c$ are reconstructed for the 2011 (2012) data. At the hardware trigger stage, events are required to have a muon with high p_T or a

hadron, photon or electron with high transverse energy in the calorimeters. The transverse energy threshold for hadrons is set at $3.5\,\mathrm{GeV}$. Signal candidates may come from events where the hardware trigger was activated either by signal particles or by other particles in the event. The proportion of events triggered by other particles in the event is found to be very similar between the signal and the normalisation decay modes in both long and downstream samples. The software trigger requires a two- or three-track secondary vertex with a significant displacement from the primary pp interaction vertices. At least one charged particle must have $p_\mathrm{T} > 1.7\,\mathrm{GeV}/c$ and be inconsistent with originating from a PV. A multivariate algorithm [12] is used for the identification of secondary vertices consistent with the decay of a b hadron to a final state of two or more particles.

The efficiency of the software trigger selection on both decay modes varied during the data-taking period. During the 2011 data taking, downstream tracks were not reconstructed in the software trigger. Such tracks were included in the trigger during the 2012 data taking and a further significant improvement in the algorithms was implemented mid-year. Consequently, the data are subdivided into three data-taking periods (2011, 2012a and 2012b) in addition to the two V^0 reconstruction categories (long and downstream). The 2012b sample has the highest trigger efficiency, especially in the downstream category, and is also the largest data set, corresponding to $1.4\,\mathrm{fb}^{-1}$ of integrated luminosity.

Simulated data samples are used to study the response of the detector and to investigate possible sources of background to the signal and the normalisation modes. The pp collisions are generated using PYTHIA [13, 14] with a specific LHCb configuration [15]. Decays of hadronic particles are described by EVTGEN [16], in which final-state radiation is generated using PHOTOS [17]. The interaction of the generated particles with the detector, and its response, are implemented using the GEANT4 toolkit [18, 19] as described in ref. [20].

3 Sample selection and composition

The selection consists of two stages, a preselection with high efficiency for the signal decays, followed by a multivariate classifier. The selection requirements of both signal and normalisation decays exploit the characteristic topology and kinematic properties of two-body decays to final states containing a V^0 hadron. The B^+ candidates are reconstructed by combining, in a good-quality vertex, a V^0 candidate with a charged particle hereafter referred to as the bachelor particle. Both the $B^+ \to p\overline{\Lambda}$ and the $B^+ \to K_\mathrm{S}^0 \pi^+$ decay chains are refitted [21] using the known Λ or K_S^0 mass [22]. The resulting B^+ invariant-mass resolutions are improved and nearly identical for the long and downstream V^0 candidates. The long and downstream samples are thus merged after full selection, thereby simplifying the extraction of the signal yields.

A minimum p_T requirement is imposed for all final-state particles. The V^0 decay products must have a large IP with respect to all PVs; hence a minimum χ^2_IP with respect to the PVs is imposed on each decay product, where χ^2_IP is defined as the difference between the vertex-fit χ^2 of a PV reconstructed with and without the track in question. The V^0 decay products are also required to form a good quality vertex. The V^0 candidate is

associated to the PV that gives the smallest $\chi^2_{\rm IP}$. The selection favours long-lived V^0 decays by requiring that the decay vertex and the associated PV are well separated.

The Λ decay products must satisfy $|m(p\pi) - m_\Lambda| < 20(15)\,{\rm MeV}/c^2$ for downstream (long) candidates, where m_Λ is the known Λ mass [22]. The corresponding criterion for the $K^0_{\rm S}$ decay products is $|m(\pi\pi) - m_{K^0_{\rm S}}| < 30(15)\,{\rm MeV}/c^2$, where $m_{K^0_{\rm S}}$ is the known $K^0_{\rm S}$ mass [22].

The B^+ candidate is required to have a small $\chi^2_{\rm IP}$ with respect to the associated PV as its reconstructed momentum vector should point to its production vertex. This pointing condition of the B^+ candidate is further reinforced by requiring that the angle between the B^+ candidate momentum vector and the line connecting the associated PV and the B^+ decay vertex (B^+ direction angle) is close to zero.

To avoid selection biases, $p\overline{\Lambda}$ candidates with invariant mass within $64\,{\rm MeV}/c^2$ (approximately four times the mass resolution) around the known B^+ mass are not examined until all analysis choices are finalised. No such procedure is applied to the spectrum of the well-known $B^+ \to K^0_{\rm S}\pi^+$ decay. The final selections of $p\overline{\Lambda}$ and $K^0_{\rm S}\pi^+$ candidates rely on artificial neural networks [23], multilayer perceptrons (MLPs), as multivariate classifiers to separate signal from background; the MLP implementation is provided by the TMVA toolkit [24].

Separate MLPs are employed for the $p\overline{\Lambda}$ and the $K^0_{\rm S}\pi^+$ selection. The MLPs are trained with simulated samples to represent the signals and with data from the high-mass sideband in the range 5350–$6420\,{\rm MeV}/c^2$ for the background, to avoid partially reconstructed backgrounds. For the well-known $K^0_{\rm S}\pi^+$ spectra both low- and high-mass sidebands are used. The training and selection is performed separately for each period of data taking (the 2012a and 2012b samples are merged) and for downstream and long samples. Optimisation biases are avoided by splitting each of these samples into three disjoint subsamples: each MLP is trained on a different subsample in such a way that events used to train one MLP are classified with another. The response of the MLPs is uncorrelated with the mass of the $p\overline{\Lambda}$ and $K^0_{\rm S}\pi^+$ final states. The MLP training relies on an accurate description of the distributions of the input variables in simulated events. The agreement between data and simulation is verified with kinematic distributions from $B^+ \to K^0_{\rm S}\pi^+$ decays, where the combinatorial background in the invariant mass spectrum is statistically suppressed using the *sPlot* technique [25]. No significant deviations are found, giving confidence that the inputs to the MLPs represent the data reliably. The variables used in the MLP classifiers are properties of the B^+ candidate and of the bachelor particle and V^0 daughters. The input variables are the following: the χ^2 per degree of freedom of the kinematic fit of the decay chain; the B^+ decay length, $\chi^2_{\rm IP}$ and direction angle; the difference between the z-positions of the B^+ and the V^0 decay vertices divided by its uncertainty squared; the bachelor particle $p_{\rm T}$; and the $p_{\rm T}$ of the V^0 decay products. Extra variables are exploited in the selection of the long samples: the $\chi^2_{\rm IP}$ of the bachelor particle and of both V^0 decay products.

In addition to the MLP selection, particle identification (PID) requirements are necessary to reject sources of background coming from B decays. A loose PID requirement is imposed on the V^0 daughters, exploiting information from the ring-imaging Cherenkov detectors, to

remove background from K_S^0 (Λ) decays in the $p\overline{\Lambda}$ ($K_S^0\pi^+$) samples. The PID selection on the bachelor particle is optimised together with the MLP selection as follows. The figure of merit $\epsilon_{\mathrm{sig}}/(a/2 + \sqrt{B_{\mathrm{exp}}})$ suggested in ref. [26] is used to determine the optimal MLP and PID requirements for each $B^+ \to p\overline{\Lambda}$ subsample separately, where ϵ_{sig} represents the combined MLP and PID selection efficiency. The term $a = 3$ quantifies the target level of significance in units of standard deviations. The expected number of background candidates, B_{exp}, within the (initially excluded) signal region is estimated by extrapolating the result of a fit to the invariant mass distribution of the data sidebands. A standard significance $S/\sqrt{S + B}$ is used to optimise the selection of the $B^+ \to K_S^0\pi^+$ candidates, where B is the number of background candidates and S the number of signal candidates in the invariant mass range $5000 - 5600\,\mathrm{MeV}/c^2$. The presence of the cross-feed background $B^+ \to K_S^0 K^+$ is taken into account. The fraction of events with more than one selected candidate is negligible; all candidates are kept.

Efficiencies are determined for each data-taking period and each V^0 reconstruction category, and subsequently combined accounting for the mixture of these subsamples in data. The efficiency of the MLP selection is determined from simulation. Large data control samples of $D^0 \to K^-\pi^+$, $\Lambda \to p\pi^-$ and $\Lambda_c^+ \to pK^-\pi^+$ decays are employed [27] to determine the efficiency of the PID requirements. All other selection efficiencies, $i.e.$ trigger, reconstruction and preselection efficiencies, are determined from simulation. The overall selection efficiencies of this analysis are of order 10^{-4}. The expected yield of the control mode $B^+ \to K_S^0\pi^+$, calculated from the product of the integrated luminosity, the $b\overline{b}$ cross-section, the b hadronisation probability, the $B^+ \to K_S^0\pi^+$ visible branching fraction and the total selection efficiency, agrees with the yield obtained from the fit to the data at the level of 1.4 standard deviations.

Possible sources of non-combinatorial background to the $p\overline{\Lambda}$ and $K_S^0\pi^+$ spectra are investigated using extensive simulation samples. These sources include partially reconstructed backgrounds in which one or more particles from the decay of a b hadron are not associated with the signal candidate, and b-hadron decays where one or more decay products are misidentified, such as decays with K_S^0 mesons misidentified as Λ baryons in the $p\overline{\Lambda}$ spectrum. The peaking background from $B^+ \to p\overline{p}\pi^+$ decays in the $p\overline{\Lambda}$ spectrum is found to be insignificant after the MLP selection. The currently unobserved $B^+ \to p\overline{\Sigma}^0$ decay is treated as a source of systematic uncertainty. The ensemble of specific backgrounds does not peak in the signal region but rather contributes a smooth $p\overline{\Lambda}$ mass spectrum, which is indistinguishable from the dominant combinatorial background.

4   Signal yield determination

The yields of the signal and background candidates in both the signal and normalisation samples are determined, after the full selection, using unbinned extended maximum likelihood fits to the invariant mass spectra. The signal lineshapes are found to be compatible between the data-taking periods and between the long and downstream categories, so all subsamples are merged together into a single spectrum.
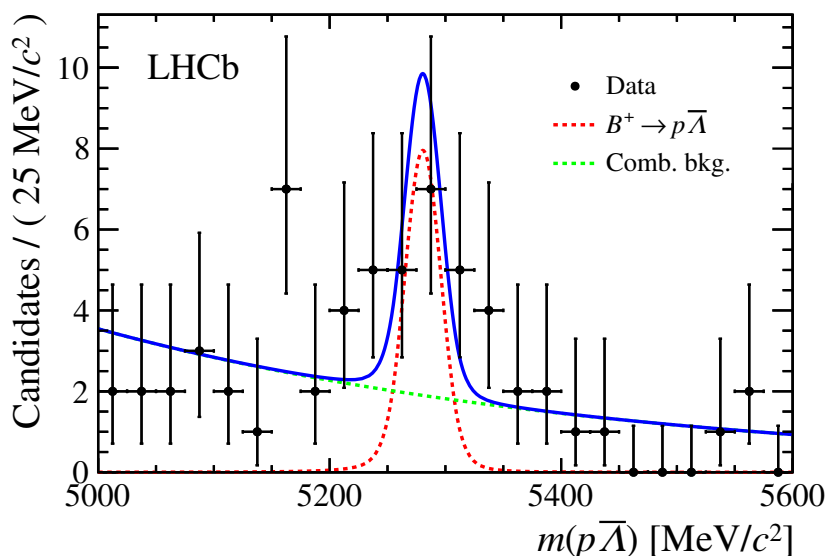
Figure 1. Invariant mass distribution of $p\overline{\Lambda}$ candidates after full selection. The result of the fit to the data (blue, solid) is shown together with each fit model component, namely the $B^+ \to p\overline{\Lambda}$ signal and the combinatorial background.

The probability density functions (PDFs) of B-meson signals have asymmetric tails that result from a combination of detector-related effects and effects of final-state radiation. The signal mass distributions are verified in simulation to be modelled accurately by the sum of two Crystal Ball (CB) functions [28] describing the high- and low-mass asymmetric tails. The peak values and the core widths of the two CB components are set to be the same.

The $p\overline{\Lambda}$ spectrum comprises the $B^+ \to p\overline{\Lambda}$ signal and combinatorial background. Contamination from partially reconstructed backgrounds, with or without misidentified particles, is treated as a source of systematic uncertainty. The peak position and tail parameters of the $B^+ \to p\overline{\Lambda}$ CB components are fixed to the values obtained from simulation. The core width parameter, also fixed, is obtained by multiplying the value from simulation by a scaling factor to account for differences in the resolution between data and simulation. This factor, determined from the $B^+ \to K^0_S \pi^+$ data and simulation samples, is compatible with unity (1.01 ± 0.06) and gives a width of approximately $16\,\text{MeV}/c^2$. The invariant mass distribution of the combinatorial background is described by an exponential function, with the slope parameter determined from the fit.

The fit to the $p\overline{\Lambda}$ invariant mass distribution, presented in figure 1, determines three parameters: two yields and the slope of the combinatorial background model. An excess of $B^+ \to p\overline{\Lambda}$ candidates with respect to background expectations is found, corresponding to a signal yield of $N(B^+ \to p\overline{\Lambda}) = 13.0^{+5.1}_{-4.3}$, where the uncertainties, obtained from a profile likelihood scan, are statistical only.

The statistical significance of the $B^+ \to p\overline{\Lambda}$ signal is determined with a large set of samples simulated assuming the presence of background only. For each simulated sample, a number of events distributed according to the exponential model of the background is
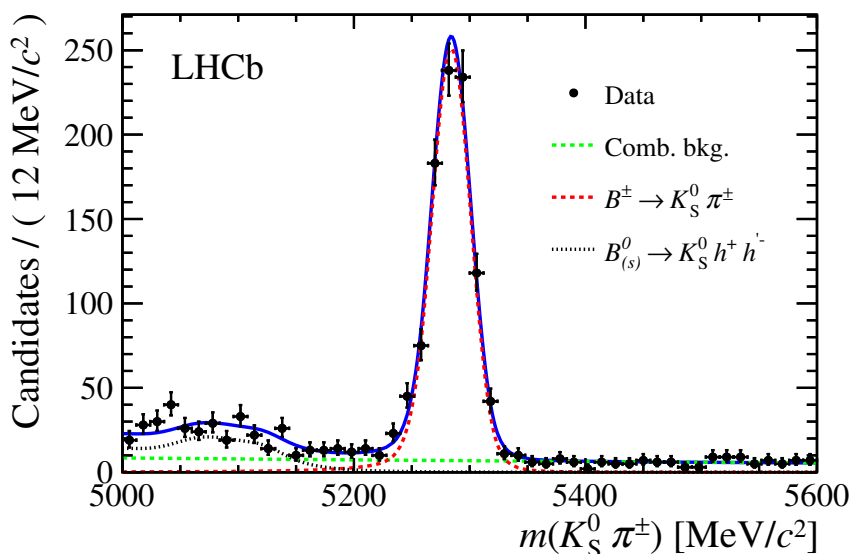
Figure 2. Invariant mass distribution of $K^0_S \pi^+$ candidates after full selection. The result of the fit to the data (blue, solid) is shown together with each fit model component, namely the $B^+ \to K^0_S \pi^+$ signal, the $B^0_{(s)} \to K^0_S h^+ h'^-$ partially reconstructed background, and the combinatorial background. The vanishingly small $B^+ \to K^0_S K^+$ misidentified cross-feed is not displayed.

drawn from a Poisson distribution with mean equal to the number of observed background events. For each sample, the log-likelihood ratio $2\ln(L_{S+B}/L_B)$ is computed, where L_{S+B} and L_B are the likelihoods from the full fit and from the fit without the signal component, respectively. The fraction of samples that yield log-likelihood ratios larger than the ratio observed in data is 3.4×10^{-5}, which corresponds to a statistical significance of 4.1 standard deviations. Inclusion of the 6.7% systematic uncertainty affecting the signal yield gives only a marginal change in the signal significance.

The $K^0_S \pi^+$ mass spectrum of the normalisation decay is described as the sum of components accounting for the $B^+ \to K^0_S \pi^+$ signal, the $B^+ \to K^0_S K^+$ misidentified background, backgrounds from partially reconstructed $B^0_{(s)} \to K^0_S h^+ h'^-$ decays ($h^{(\prime)} = \pi, K$), and combinatorial background. Any contamination from other decays is treated as a source of systematic uncertainty.

The $B^+ \to K^0_S h^+$ CB tail parameters and the relative normalisation of the two CB functions are fixed to the values obtained from simulation. The mean and the width (approximately $17\,\mathrm{MeV}/c^2$) of the $B^+ \to K^0_S \pi^+$ peak are allowed to vary in the fit to the data, whilst they are fixed for the very small $B^+ \to K^0_S K^+$ peak contribution. The mean of the $B^+ \to K^0_S K^+$ peak, around $5240\,\mathrm{MeV}/c^2$, is fixed using the mass difference between the $B^+ \to K^0_S K^+$ and $B^+ \to K^0_S \pi^+$ peaks obtained from simulation. The $B^+ \to K^0_S K^+$ yield is Gaussian constrained using the $B^+ \to K^0_S \pi^+$ yield, taking into account the differences in branching fraction and selection efficiency.

The partially reconstructed backgrounds that populate the lower-mass sideband are assumed to arise from the $B^0_{(s)} \to K^0_S h^+ h'^-$ decay modes with the largest branching fractions, namely $B^0 \to K^0_S \pi^+ \pi^-$, $B^0 \to K^0_S K^+ K^-$, $B^0_s \to K^0_S \pi^+ \pi^-$ and $B^0_s \to K^0_S K^\pm \pi^\mp$ [29].

Source	Value [%]	
	$B^+ \to p\overline{\Lambda}$	$B^+ \to K_S^0 \pi^+$
$\mathcal{B}(B^+ \to K_S^0 \pi^+)$	—	3.2
Trigger efficiencies ratio	3.5	—
Selection efficiencies ratio	2.2	—
PID uncertainties	1.2	3.5
Tracking efficiencies ratio	6.0	—
Yields from mass fits	6.7	3.0
Simulation statistics	1.7	3.3
Total	10.1	6.5

Table 1. Summary of systematic uncertainties relative to the measured $B^+ \to p\overline{\Lambda}$ branching fraction. The contributions are split into those that come from the signal decay and those that come from the normalisation decay. The total corresponds to the sum of all contributions added in quadrature.

Only $B^0 \to K_S^0 \pi^+ \pi^-$, $B_s^0 \to K_S^0 \pi^+ \pi^-$ and $B_s^0 \to K_S^0 K^{\pm} \pi^{\mp}$ are considered given that $B^0 \to K_S^0 K^+ K^-$ is further suppressed because of a low kaon-to-pion misidentification probability. The overall shape of the $B_{(s)}^0 \to K_S^0 h^+ h'^-$ decay modes in the $K_S^0 \pi^+$ mass spectrum is obtained from simulation accounting for the relative yields related to different B-meson fragmentation probabilities, selection efficiencies and branching fractions. The invariant mass distribution of the combinatorial background is described by an exponential function, with the slope parameter determined from the mass fit.

The resulting spectrum shows a prominent $B^+ \to K_S^0 \pi^+$ peak above little combinatorial and partially reconstructed background. The fit to the $K_S^0 \pi^+$ spectrum, presented in figure 2, determines seven parameters: three shape parameters and four yields. The signal yield obtained is $N(B^+ \to K_S^0 \pi^+) = 930 \pm 34$, where the uncertainty is statistical only.

5 Systematic uncertainties

The systematic uncertainties are reduced by performing the branching fraction measurement relative to a decay mode topologically identical to the decay of interest. Uncertainties arise from imperfect knowledge of the selection efficiencies, systematic uncertainties on the fitted yields, and uncertainties on the branching fractions of decays involved in the calculation of the $B^+ \to p\overline{\Lambda}$ branching fraction. The systematic uncertainties assigned to the measurement of the $B^+ \to p\overline{\Lambda}$ branching fraction are summarised in table 1.

The uncertainty on the branching fraction of the normalisation channel, $\mathcal{B}(B^+ \to K_S^0 \pi^+) = (11.895 \pm 0.375) \times 10^{-6}$ [30] (assuming that half of the K^0 mesons decay as a K_S^0), is taken as a systematic uncertainty. The uncertainties on the branching fractions $\mathcal{B}(\Lambda \to p\pi^-) = (63.9 \pm 0.5)\%$ and $\mathcal{B}(K_S^0 \to \pi^+ \pi^-) = (69.20 \pm 0.05)\%$ are accounted for, but omitted from the table as they are negligible compared to all other sources of systematic uncertainty.

The determination of the selection efficiencies entails several sources of systematic uncertainty. A systematic uncertainty is assigned to take into account possible differences in the trigger efficiencies between data and simulation, following the procedure and studies

described in ref. [31]. The $B^+ \to K_S^0 \pi^+$ mode is used as a proxy for the assessment of the systematic uncertainties related to the MLP selection. Distributions for the $B^+ \to K_S^0 \pi^+$ MLP input variables are obtained from data using the *sPlot* technique. The distributions from simulation showing the largest discrepancies are weighted to match those of the data. The selection efficiencies are recalculated with the same MLPs, but using the weighted distributions, to derive the variations in efficiency, and hence the systematic uncertainty on the selection. The uncertainty associated with the imperfect knowledge of PID selection efficiencies is assessed varying the binning of the PID control samples in track momentum and pseudorapidity, and also accounting for a dependence of the efficiency on the event track multiplicity after weighting the distribution of the latter to match that of the data. The two uncertainties are combined in quadrature.

The signal decay has two baryons in the final state whilst only mesons are present in the final state of the normalisation channel. Tracking efficiency uncertainties do not cancel fully in this instance. The degree to which the simulation describes the hadronic interactions with the material is less accurate for baryons than it is for mesons. A systematic uncertainty of 4% per proton is estimated whereas the corresponding uncertainty is 1.5% for pions and kaons [32]. A non-negligible systematic uncertainty on the tracking efficiencies as calculated from simulation, including correlations, results from these sources of uncertainty.

Systematic uncertainties on the fit yields arise from potential mismodelling of the fit components and from the uncertainties on the values of the parameters fixed in the fits. They are investigated using data and by studying a large number of simulated data samples, with parameters varying within their estimated uncertainties. Changing the combinatorial background model to a linear shape decreases the signal yield by 4.6%, with no significant effect on the signal significance and the final result. Possible contamination from the unobserved decay $B^+ \to p\overline{\Sigma}^0$ is studied by adding such a component. The fitted $B^+ \to p\overline{\Sigma}^0$ yield is found to be compatible with zero, and the shift in the $B^+ \to p\overline{\Lambda}$ yield with respect to the nominal yield is taken as a systematic uncertainty.

The finite size of the simulation samples used in the analysis further contributes as a source of systematic uncertainty. The total systematic uncertainty on the $B^+ \to p\overline{\Lambda}$ branching fraction is given by the sum of all contributions added in quadrature, amounting to 12.0%.

6 Results and conclusion

The $B^+ \to p\overline{\Lambda}$ branching fraction is determined relative to that of the $B^+ \to K_S^0 \pi^+$ normalisation channel according to

$$\mathcal{B}(B^+ \to p\overline{\Lambda}) = \frac{N(B^+ \to p\overline{\Lambda})}{N(B^+ \to K_S^0 \pi^+)} \frac{\epsilon_{B^+ \to K_S^0 \pi^+}}{\epsilon_{B^+ \to p\overline{\Lambda}}} \frac{\mathcal{B}(K_S^0 \to \pi^+ \pi^-)}{\mathcal{B}(\Lambda \to p\pi^-)} \mathcal{B}(B^+ \to K_S^0 \pi^+),$$

where N represent the yields determined from the mass fits and ϵ are the selection efficiencies. It is measured to be

$$\mathcal{B}(B^+ \to p\overline{\Lambda}) = (2.4 \,^{+1.0}_{-0.8} \pm 0.3) \times 10^{-7},$$

where the first uncertainty is statistical and the second systematic.

In summary, a search is reported for the rare two-body charmless baryonic decay $B^+ \to p\overline{\Lambda}$ using a pp collision data sample collected by the LHCb experiment at centre-of-mass energies of 7 and 8 TeV, corresponding to an integrated luminosity of $3\,\text{fb}^{-1}$. An excess of $B^+ \to p\overline{\Lambda}$ candidates with respect to background expectations is found with a statistical significance of 4.1 standard deviations. This is the first evidence for this decay process.

The measured branching fraction is compatible with the theoretical predictions in refs. [5, 6] but is in tension with calculations based on QCD sum rules [4] and calculations based on factorisation with the hypothesis of the violation of partial conservation of the axial-vector current at the GeV scale [7]. It helps shed light on an area of hadronic physics in which experimental input is needed, namely the study of the mechanisms responsible for decays of B mesons to baryonic final states.

Acknowledgments

References

[1] BELLE, BABAR collaboration, A.J. Bevan et al., *The physics of the B factories*, *Eur. Phys. J.* **C 74** (2014) 3026 [arXiv:1406.6311] [INSPIRE].

[2] LHCb collaboration, *Evidence of CP violation in $B^+ \to p\bar{p}K^+$ decays*, *Phys. Rev. Lett.* **113** (2014) 141801 [arXiv:1407.5907] [LHCb-PAPER-2014-034].

[3] LHCb collaboration, *First evidence for the two-body charmless baryonic decay $B^0 \to p\bar{p}$*, *JHEP* **10** (2013) 055 [arXiv:1308.0961] [LHCb-PAPER-2013-038].

[4] V.L. Chernyak and I.R. Zhitnitsky, *B meson exclusive decays into baryons*, *Nucl. Phys.* **B 345** (1990) 137 [INSPIRE].

[5] H.-Y. Cheng and K.-C. Yang, *Charmless exclusive baryonic B decays*, *Phys. Rev.* **D 66** (2002) 014020 [hep-ph/0112245] [INSPIRE].

[6] C.-K. Chua, *Charmless two-body baryonic $B_{u,d,s}$ decays revisited*, *Phys. Rev.* **D 89** (2014) 056003 [arXiv:1312.2335] [INSPIRE].

[7] Y.K. Hsiao and C.Q. Geng, *Violation of partial conservation of the axial-vector current and two-body baryonic B and D_s decays*, *Phys. Rev.* **D 91** (2015) 077501 [arXiv:1407.7639] [INSPIRE].

[8] CLEO collaboration, T.E. Coan et al., *Search for exclusive rare baryonic decays of B mesons*, *Phys. Rev.* **D 59** (1999) 111101 [hep-ex/9810043] [INSPIRE].

[9] BELLE collaboration, Y.-T. Tsai et al., *Search for $B^0 \to p\bar{p}$, $\Lambda\bar{\Lambda}$ and $B^+ \to p\bar{\Lambda}$ at Belle*, *Phys. Rev.* **D 75** (2007) 111101 [hep-ex/0703048] [INSPIRE].

[10] LHCb collaboration, *The LHCb detector at the LHC*, 2008 *JINST* **3** S08005 [INSPIRE].

[11] LHCb collaboration, *LHCb detector performance*, *Int. J. Mod. Phys.* **A 30** (2015) 1530022 [arXiv:1412.6352] [INSPIRE].

[12] V.V. Gligorov and M. Williams, *Efficient, reliable and fast high-level triggering using a bonsai boosted decision tree*, 2013 *JINST* **8** P02013 [arXiv:1210.6861] [INSPIRE].

[13] T. Sjöstrand, S. Mrenna and P.Z. Skands, *PYTHIA 6.4 physics and manual*, *JHEP* **05** (2006) 026 [hep-ph/0603175] [INSPIRE].

[14] T. Sjöstrand, S. Mrenna and P.Z. Skands, *A brief introduction to PYTHIA 8.1*, *Comput. Phys. Commun.* **178** (2008) 852 [arXiv:0710.3820] [INSPIRE].

[15] I. Belyaev et al., *Handling of the generation of primary events in Gauss, the LHCb simulation framework*, *J. Phys. Conf. Ser.* **331** (2011) 032047 [INSPIRE].

[16] D.J. Lange, *The EvtGen particle decay simulation package*, *Nucl. Instrum. Meth.* **A 462** (2001) 152 [INSPIRE].

[17] P. Golonka and Z. Was, *PHOTOS Monte Carlo: a precision tool for QED corrections in Z and W decays*, *Eur. Phys. J.* **C 45** (2006) 97 [hep-ph/0506026] [INSPIRE].

[18] GEANT4 collaboration, J. Allison et al., *Geant4 developments and applications*, *IEEE Trans. Nucl. Sci.* **53** (2006) 270.

[19] GEANT4 collaboration, S. Agostinelli et al., *Geant4 — A simulation toolkit*, *Nucl. Instrum. Meth.* **A 506** (2003) 250 [INSPIRE].

[20] M. Clemencic et al., *The LHCb simulation application, Gauss: design, evolution and experience*, *J. Phys. Conf. Ser.* **331** (2011) 032023 [INSPIRE].

[21] W.D. Hulsbergen, *Decay chain fitting with a Kalman filter*, *Nucl. Instrum. Meth.* **A 552** (2005) 566 [physics/0503191] [INSPIRE].

[22] PARTICLE DATA GROUP, K.A. Olive et al., *Review of particle physics*, *Chin. Phys.* **C 38** (2014) 090001 [INSPIRE].

[23] D.E. Rumelhart, G.E. Hinton and R.J. Williams, *Parallel distributed processing: explorations in the microstructure of cognition*, volume 1, MIT, Cambridge, U.S.A. (1986).

[24] A. Hoecker et al., *TMVA — Toolkit for MultiVariate data Analysis with ROOT*, PoS(ACAT)040 [physics/0703039] [INSPIRE].

[25] M. Pivk and F.R. Le Diberder, *SPlot: a statistical tool to unfold data distributions*, *Nucl. Instrum. Meth.* **A 555** (2005) 356 [physics/0402083] [INSPIRE].

[26] G. Punzi, *Sensitivity of searches for new signals and its optimization*, *eConf* **C 030908** (2003) MODT002 [physics/0308063] [INSPIRE].

[27] M. Adinolfi et al., *Performance of the LHCb RICH detector at the LHC*, *Eur. Phys. J.* **C 73** (2013) 2431 [arXiv:1211.6759] [INSPIRE].

[28] T. Skwarnicki, *A study of the radiative cascade transitions between the Υ' and Υ resonances*, Ph.D. thesis, Institute of Nuclear Physics, Krakow, Poland (1986).

[29] LHCb collaboration, *Study of $B^0_{(s)} \to K^0_S h^+ h'^-$ decays with first observation of $B^0_s \to K^0_S K^\pm \pi^\mp$ and $B^0_s \to K^0_S \pi^+ \pi^-$*, *JHEP* **10** (2013) 143 [arXiv:1307.7648] [CERN-PH-EP-2013-139].

[30] HEAVY FLAVOR AVERAGING GROUP (HFAG) collaboration, Y. Amhis et al., *Averages of b-hadron, c-hadron and τ-lepton properties as of summer 2014*, arXiv:1412.7515 [INSPIRE].

[31] LHCb collaboration, *Observation of the $\Lambda^0_b \to \Lambda \phi$ decay*, *Phys. Lett.* **B 759** (2016) 282 [arXiv:1603.02870] [LHCb-PAPER-2016-002].

[32] LHCb collaboration, *Measurement of the track reconstruction efficiency at LHCb*, 2015 *JINST* **10** P02007 [arXiv:1408.1251] [INSPIRE].

The LHCb collaboration

R. Aaij[40], B. Adeva[39], M. Adinolfi[48], Z. Ajaltouni[5], S. Akar[6], J. Albrecht[10], F. Alessio[40],
M. Alexander[53], S. Ali[43], G. Alkhazov[31], P. Alvarez Cartelle[55], A.A. Alves Jr[59], S. Amato[2],
S. Amerio[23], Y. Amhis[7], L. An[41], L. Anderlini[18], G. Andreassi[41], M. Andreotti[17,g], J.E. Andrews[60],
R.B. Appleby[56], F. Archilli[43], P. d'Argent[12], J. Arnau Romeu[6], A. Artamonov[37], M. Artuso[61],
E. Aslanides[6], G. Auriemma[26], M. Baalouch[5], I. Babuschkin[56], S. Bachmann[12], J.J. Back[50],
A. Badalov[38], C. Baesso[62], S. Baker[55], W. Baldini[17], R.J. Barlow[56], C. Barschel[40], S. Barsuk[7],
W. Barter[40], M. Baszczyk[27], V. Batozskaya[29], B. Batsukh[61], V. Battista[41], A. Bay[41],
L. Beaucourt[4], J. Beddow[53], F. Bedeschi[24], I. Bediaga[1], L.J. Bel[43], V. Bellee[41], N. Belloli[21,i],
K. Belous[37], I. Belyaev[32], E. Ben-Haim[8], G. Bencivenni[19], S. Benson[43], J. Benton[48],
A. Berezhnoy[33], R. Bernet[42], A. Bertolin[23], C. Betancourt[42], F. Betti[15], M.-O. Bettler[40],
M. van Beuzekom[43], Ia. Bezshyiko[42], S. Bifani[47], P. Billoir[8], T. Bird[56], A. Birnkraut[10],
A. Bitadze[56], A. Bizzeti[18,u], T. Blake[50], F. Blanc[41], J. Blouw[11,†], S. Blusk[61], V. Bocci[26],
T. Boettcher[58], A. Bondar[36,w], N. Bondar[31,40], W. Bonivento[16], I. Bordyuzhin[32], A. Borgheresi[21,i],
S. Borghi[56], M. Borisyak[35], M. Borsato[39], F. Bossu[7], M. Boubdir[9], T.J.V. Bowcock[54], E. Bowen[42],
C. Bozzi[17,40], S. Braun[12], M. Britsch[12], T. Britton[61], J. Brodzicka[56], E. Buchanan[48], C. Burr[56],
A. Bursche[2], J. Buytaert[40], S. Cadeddu[16], R. Calabrese[17,g], M. Calvi[21,i], M. Calvo Gomez[38,m],
A. Camboni[38], P. Campana[19], D.H. Campora Perez[40], L. Capriotti[56], A. Carbone[15,e],
G. Carboni[25,j], R. Cardinale[20,h], A. Cardini[16], P. Carniti[21,i], L. Carson[52], K. Carvalho Akiba[2],
G. Casse[54], L. Cassina[21,i], L. Castillo Garcia[41], M. Cattaneo[40], Ch. Cauet[10], G. Cavallero[20],
R. Cenci[24,t], D. Chamont[7], M. Charles[8], Ph. Charpentier[40], G. Chatzikonstantinidis[47],
M. Chefdeville[4], S. Chen[56], S.-F. Cheung[57], V. Chobanova[39], M. Chrzaszcz[42,27], X. Cid Vidal[39],
G. Ciezarek[43], P.E.L. Clarke[52], M. Clemencic[40], H.V. Cliff[49], J. Closier[40], V. Coco[59], J. Cogan[6],
E. Cogneras[5], V. Cogoni[16,40,f], L. Cojocariu[30], G. Collazuol[23,o], P. Collins[40],
A. Comerma-Montells[12], A. Contu[40], A. Cook[48], G. Coombs[40], S. Coquereau[38], G. Corti[40],
M. Corvo[17,g], C.M. Costa Sobral[50], B. Couturier[40], G.A. Cowan[52], D.C. Craik[52], A. Crocombe[50],
M. Cruz Torres[62], S. Cunliffe[55], R. Currie[55], C. D'Ambrosio[40], F. Da Cunha Marinho[2],
E. Dall'Occo[43], J. Dalseno[48], P.N.Y. David[43], A. Davis[59], O. De Aguiar Francisco[2], K. De Bruyn[6],
S. De Capua[56], M. De Cian[12], J.M. De Miranda[1], L. De Paula[2], M. De Serio[14,d], P. De Simone[19],
C.-T. Dean[53], D. Decamp[4], M. Deckenhoff[10], L. Del Buono[8], M. Demmer[10], A. Dendek[28],
D. Derkach[35], O. Deschamps[5], F. Dettori[40], B. Dey[22], A. Di Canto[40], H. Dijkstra[40], F. Dordei[40],
M. Dorigo[41], A. Dosil Suárez[39], A. Dovbnya[45], K. Dreimanis[54], L. Dufour[43], G. Dujany[56],
K. Dungs[40], P. Durante[40], R. Dzhelyadin[37], A. Dziurda[40], A. Dzyuba[31], N. Déléage[4], S. Easo[51],
M. Ebert[52], U. Egede[55], V. Egorychev[32], S. Eidelman[36,w], S. Eisenhardt[52], U. Eitschberger[10],
R. Ekelhof[10], L. Eklund[53], S. Ely[61], S. Esen[12], H.M. Evans[49], T. Evans[57], A. Falabella[15],
N. Farley[47], S. Farry[54], R. Fay[54], D. Fazzini[21,i], D. Ferguson[52], A. Fernandez Prieto[39],
F. Ferrari[15,40], F. Ferreira Rodrigues[2], M. Ferro-Luzzi[40], S. Filippov[34], R.A. Fini[14], M. Fiore[17,g],
M. Fiorini[17,g], M. Firlej[28], C. Fitzpatrick[41], T. Fiutowski[28], F. Fleuret[7,b], K. Fohl[40],
M. Fontana[16,40], F. Fontanelli[20,h], D.C. Forshaw[61], R. Forty[40], V. Franco Lima[54], M. Frank[40],
C. Frei[40], J. Fu[22,q], W. Funk[40], E. Furfaro[25,j], C. Färber[40], A. Gallas Torreira[39], D. Galli[15,e],
S. Gallorini[23], S. Gambetta[52], M. Gandelman[2], P. Gandini[57], Y. Gao[3], L.M. Garcia Martin[69],
J. García Pardiñas[39], J. Garra Tico[49], L. Garrido[38], P.J. Garsed[49], D. Gascon[38], C. Gaspar[40],
L. Gavardi[10], G. Gazzoni[5], D. Gerick[12], E. Gersabeck[12], M. Gersabeck[56], T. Gershon[50], Ph. Ghez[4],
S. Gianì[41], V. Gibson[49], O.G. Girard[41], L. Giubega[30], K. Gizdov[52], V.V. Gligorov[8], D. Golubkov[32],
A. Golutvin[55,40], A. Gomes[1,a], I.V. Gorelov[33], C. Gotti[21,i], M. Grabalosa Gándara[5],
R. Graciani Diaz[38], L.A. Granado Cardoso[40], E. Graugés[38], E. Graverini[42], G. Graziani[18],
A. Grecu[30], P. Griffith[47], L. Grillo[21,40,i], B.R. Gruberg Cazon[57], O. Grünberg[67], E. Gushchin[34],

Yu. Guz[37], T. Gys[40], C. Göbel[62], T. Hadavizadeh[57], C. Hadjivasiliou[5], G. Haefeli[41], C. Haen[40],
S.C. Haines[49], S. Hall[55], B. Hamilton[60], X. Han[12], S. Hansmann-Menzemer[12], N. Harnew[57],
S.T. Harnew[48], J. Harrison[56], M. Hatch[40], J. He[63], T. Head[41], A. Heister[9], K. Hennessy[54],
P. Henrard[5], L. Henry[8], E. van Herwijnen[40], M. Heß[67], A. Hicheur[2], D. Hill[57], C. Hombach[56],
H. Hopchev[41], W. Hulsbergen[43], T. Humair[55], M. Hushchyn[35], N. Hussain[57], D. Hutchcroft[54],
M. Idzik[28], P. Ilten[58], R. Jacobsson[40], A. Jaeger[12], J. Jalocha[57], E. Jans[43], A. Jawahery[60],
F. Jiang[3], M. John[57], D. Johnson[40], C.R. Jones[49], C. Joram[40], B. Jost[40], N. Jurik[57],
S. Kandybei[45], W. Kanso[6], M. Karacson[40], J.M. Kariuki[48], S. Karodia[53], M. Kecke[12], M. Kelsey[61],
M. Kenzie[49], T. Ketel[44], E. Khairullin[35], B. Khanji[12], C. Khurewathanakul[41], T. Kirn[9],
S. Klaver[56], K. Klimaszewski[29], S. Koliiev[46], M. Kolpin[12], I. Komarov[41], R.F. Koopman[44],
P. Koppenburg[43], A. Kosmyntseva[32], A. Kozachuk[33], M. Kozeiha[5], L. Kravchuk[34], K. Kreplin[12],
M. Kreps[50], P. Krokovny[36,w], F. Kruse[10], W. Krzemien[29], W. Kucewicz[27,l], M. Kucharczyk[27],
V. Kudryavtsev[36,w], A.K. Kuonen[41], K. Kurek[29], T. Kvaratskheliya[32,40], D. Lacarrere[40],
G. Lafferty[56], A. Lai[16], G. Lanfranchi[19], C. Langenbruch[9], T. Latham[50], C. Lazzeroni[47],
R. Le Gac[6], J. van Leerdam[43], A. Leflat[33,40], J. Lefrançois[7], R. Lefèvre[5], F. Lemaitre[40],
E. Lemos Cid[39], O. Leroy[6], T. Lesiak[27], B. Leverington[12], T. Li[3], Y. Li[7], T. Likhomanenko[35,68],
R. Lindner[40], C. Linn[40], F. Lionetto[42], X. Liu[3], D. Loh[50], I. Longstaff[53], J.H. Lopes[2],
D. Lucchesi[23,o], M. Lucio Martinez[39], H. Luo[52], A. Lupato[23], E. Luppi[17,g], O. Lupton[57],
A. Lusiani[24], X. Lyu[63], F. Machefert[7], F. Maciuc[30], O. Maev[31], K. Maguire[56], S. Malde[57],
A. Malinin[68], T. Maltsev[36], G. Manca[7], G. Mancinelli[6], P. Manning[61], J. Maratas[5,v],
J.F. Marchand[4], U. Marconi[15], C. Marin Benito[38], P. Marino[24,t], J. Marks[12], G. Martellotti[26],
M. Martin[6], M. Martinelli[41], D. Martinez Santos[39], F. Martinez Vidal[69], D. Martins Tostes[2],
L.M. Massacrier[7], A. Massafferri[1], R. Matev[40], A. Mathad[50], Z. Mathe[40], C. Matteuzzi[21],
A. Mauri[42], E. Maurice[7,b], B. Maurin[41], A. Mazurov[47], M. McCann[55], J. McCarthy[47], A. McNab[56],
R. McNulty[13], B. Meadows[59], F. Meier[10], M. Meissner[12], D. Melnychuk[29], M. Merk[43], A. Merli[22,q],
E. Michielin[23], D.A. Milanes[66], M.-N. Minard[4], D.S. Mitzel[12], A. Mogini[8], J. Molina Rodriguez[1],
I.A. Monroy[66], S. Monteil[5], M. Morandin[23], P. Morawski[28], A. Mordà[6], M.J. Morello[24,t],
J. Moron[28], A.B. Morris[52], R. Mountain[61], F. Muheim[52], M. Mulder[43], M. Mussini[15], D. Müller[56],
J. Müller[10], K. Müller[42], V. Müller[10], P. Naik[48], T. Nakada[41], R. Nandakumar[51], A. Nandi[57],
I. Nasteva[2], M. Needham[52], N. Neri[22], S. Neubert[12], N. Neufeld[40], M. Neuner[12], T.D. Nguyen[41],
C. Nguyen-Mau[41,n], S. Nieswand[9], R. Niet[10], N. Nikitin[33], T. Nikodem[12], A. Novoselov[37],
D.P. O'Hanlon[50], A. Oblakowska-Mucha[28], V. Obraztsov[37], S. Ogilvy[19], R. Oldeman[16,f],
C.J.G. Onderwater[70], J.M. Otalora Goicochea[2], A. Otto[40], P. Owen[42], A. Oyanguren[69], P.R. Pais[41],
A. Palano[14,d], F. Palombo[22,q], M. Palutan[19], J. Panman[40], A. Papanestis[51], M. Pappagallo[14,d],
L.L. Pappalardo[17,g], W. Parker[60], C. Parkes[56], G. Passaleva[18], A. Pastore[14,d], G.D. Patel[54],
M. Patel[55], C. Patrignani[15,e], A. Pearce[56,51], A. Pellegrino[43], G. Penso[26], M. Pepe Altarelli[40],
S. Perazzini[40], P. Perret[5], L. Pescatore[47], K. Petridis[48], A. Petrolini[20,h], A. Petrov[68],
M. Petruzzo[22,q], E. Picatoste Olloqui[38], B. Pietrzyk[4], M. Pikies[27], D. Pinci[26], A. Pistone[20],
A. Piucci[12], V. Placinta[30], S. Playfer[52], M. Plo Casasus[39], T. Poikela[40], F. Polci[8], A. Poluektov[50,36],
I. Polyakov[61], E. Polycarpo[2], G.J. Pomery[48], A. Popov[37], D. Popov[11,40], B. Popovici[30],
S. Poslavskii[37], C. Potterat[2], E. Price[48], J.D. Price[54], J. Prisciandaro[39,40], A. Pritchard[54],
C. Prouve[48], V. Pugatch[46], A. Puig Navarro[42], G. Punzi[24,p], W. Qian[57], R. Quagliani[7,48],
B. Rachwal[27], J.H. Rademacker[48], M. Rama[24], M. Ramos Pernas[39], M.S. Rangel[2], I. Raniuk[45],
F. Ratnikov[35], G. Raven[44], F. Redi[55], S. Reichert[10], A.C. dos Reis[1], C. Remon Alepuz[69],
V. Renaudin[7], S. Ricciardi[51], S. Richards[48], M. Rihl[40], K. Rinnert[54], V. Rives Molina[38],
P. Robbe[7,40], A.B. Rodrigues[1], E. Rodrigues[59], J.A. Rodriguez Lopez[66], P. Rodriguez Perez[56,†],
A. Rogozhnikov[35], S. Roiser[40], A. Rollings[57], V. Romanovskiy[37], A. Romero Vidal[39],
J.W. Ronayne[13], M. Rotondo[19], M.S. Rudolph[61], T. Ruf[40], P. Ruiz Valls[69], J.J. Saborido Silva[39],

E. Sadykhov[32], N. Sagidova[31], B. Saitta[16,f], V. Salustino Guimaraes[1], C. Sanchez Mayordomo[69],
B. Sanmartin Sedes[39], R. Santacesaria[26], C. Santamarina Rios[39], M. Santimaria[19], E. Santovetti[25,j],
A. Sarti[19,k], C. Satriano[26,s], A. Satta[25], D.M. Saunders[48], D. Savrina[32,33], S. Schael[9],
M. Schellenberg[10], M. Schiller[53], H. Schindler[40], M. Schlupp[10], M. Schmelling[11], T. Schmelzer[10],
B. Schmidt[40], O. Schneider[41], A. Schopper[40], K. Schubert[10], M. Schubiger[41], M.-H. Schune[7],
R. Schwemmer[40], B. Sciascia[19], A. Sciubba[26,k], A. Semennikov[32], A. Sergi[47], N. Serra[42],
J. Serrano[6], L. Sestini[23], P. Seyfert[21], M. Shapkin[37], I. Shapoval[45], Y. Shcheglov[31], T. Shears[54],
L. Shekhtman[36,w], V. Shevchenko[68], B.G. Siddi[17,40], R. Silva Coutinho[42], L. Silva de Oliveira[2],
G. Simi[23,o], S. Simone[14,d], M. Sirendi[49], N. Skidmore[48], T. Skwarnicki[61], E. Smith[55], I.T. Smith[52],
J. Smith[49], M. Smith[55], H. Snoek[43], l. Soares Lavra[1], M.D. Sokoloff[59], F.J.P. Soler[53],
B. Souza De Paula[2], B. Spaan[10], P. Spradlin[53], S. Sridharan[40], F. Stagni[40], M. Stahl[12], S. Stahl[40],
P. Stefko[41], S. Stefkova[55], O. Steinkamp[42], S. Stemmle[12], O. Stenyakin[37], S. Stevenson[57],
S. Stoica[30], S. Stone[61], B. Storaci[42], S. Stracca[24,p], M. Straticiuc[30], U. Straumann[42], L. Sun[64],
W. Sutcliffe[55], K. Swientek[28], V. Syropoulos[44], M. Szczekowski[29], T. Szumlak[28], S. T'Jampens[4],
A. Tayduganov[6], T. Tekampe[10], G. Tellarini[17,g], F. Teubert[40], E. Thomas[40], J. van Tilburg[43],
M.J. Tilley[55], V. Tisserand[4], M. Tobin[41], S. Tolk[49], L. Tomassetti[17,g], D. Tonelli[40],
S. Topp-Joergensen[57], F. Toriello[61], E. Tournefier[4], S. Tourneur[41], K. Trabelsi[41], M. Traill[53],
M.T. Tran[41], M. Tresch[42], A. Trisovic[40], A. Tsaregorodtsev[6], P. Tsopelas[43], A. Tully[49],
N. Tuning[43], A. Ukleja[29], A. Ustyuzhanin[35], U. Uwer[12], C. Vacca[16,f], V. Vagnoni[15,40], A. Valassi[40],
S. Valat[40], G. Valenti[15], A. Vallier[7], R. Vazquez Gomez[19], P. Vazquez Regueiro[39], S. Vecchi[17],
M. van Veghel[43], J.J. Velthuis[48], M. Veltri[18,r], G. Veneziano[57], A. Venkateswaran[61], M. Vernet[5],
M. Vesterinen[12], B. Viaud[7], D. Vieira[1], M. Vieites Diaz[39], H. Viemann[67], X. Vilasis-Cardona[38,m],
M. Vitti[49], V. Volkov[33], A. Vollhardt[42], B. Voneki[40], A. Vorobyev[31], V. Vorobyev[36,w], C. Voß[67],
J.A. de Vries[43], C. Vázquez Sierra[39], R. Waldi[67], C. Wallace[50], R. Wallace[13], J. Walsh[24], J. Wang[61],
D.R. Ward[49], H.M. Wark[54], N.K. Watson[47], D. Websdale[55], A. Weiden[42], M. Whitehead[40],
J. Wicht[50], G. Wilkinson[57,40], M. Wilkinson[61], M. Williams[40], M.P. Williams[47], M. Williams[58],
T. Williams[47], F.F. Wilson[51], J. Wimberley[60], J. Wishahi[10], W. Wislicki[29], M. Witek[27],
G. Wormser[7], S.A. Wotton[49], K. Wraight[53], K. Wyllie[40], Y. Xie[65], Z. Xing[61], Z. Xu[41], Z. Yang[3],
Y. Yao[61], H. Yin[65], J. Yu[65], X. Yuan[36,w], O. Yushchenko[37], K.A. Zarebski[47], M. Zavertyaev[11,c],
L. Zhang[3], Y. Zhang[7], Y. Zhang[63], A. Zhelezov[12], Y. Zheng[63], X. Zhu[3], V. Zhukov[9], S. Zucchelli[15]

1 Centro Brasileiro de Pesquisas Físicas (CBPF), Rio de Janeiro, Brazil
2 Universidade Federal do Rio de Janeiro (UFRJ), Rio de Janeiro, Brazil
3 Center for High Energy Physics, Tsinghua University, Beijing, China
4 LAPP, Université Savoie Mont-Blanc, CNRS/IN2P3, Annecy-Le-Vieux, France
5 Clermont Université, Université Blaise Pascal, CNRS/IN2P3, LPC, Clermont-Ferrand, France
6 CPPM, Aix-Marseille Université, CNRS/IN2P3, Marseille, France
7 LAL, Université Paris-Sud, CNRS/IN2P3, Orsay, France
8 LPNHE, Université Pierre et Marie Curie, Université Paris Diderot, CNRS/IN2P3, Paris, France
9 I. Physikalisches Institut, RWTH Aachen University, Aachen, Germany
10 Fakultät Physik, Technische Universität Dortmund, Dortmund, Germany
11 Max-Planck-Institut für Kernphysik (MPIK), Heidelberg, Germany
12 Physikalisches Institut, Ruprecht-Karls-Universität Heidelberg, Heidelberg, Germany
13 School of Physics, University College Dublin, Dublin, Ireland
14 Sezione INFN di Bari, Bari, Italy
15 Sezione INFN di Bologna, Bologna, Italy
16 Sezione INFN di Cagliari, Cagliari, Italy
17 Sezione INFN di Ferrara, Ferrara, Italy
18 Sezione INFN di Firenze, Firenze, Italy

[19] *Laboratori Nazionali dell'INFN di Frascati, Frascati, Italy*

[20] *Sezione INFN di Genova, Genova, Italy*

[21] *Sezione INFN di Milano Bicocca, Milano, Italy*

[22] *Sezione INFN di Milano, Milano, Italy*

[23] *Sezione INFN di Padova, Padova, Italy*

[24] *Sezione INFN di Pisa, Pisa, Italy*

[25] *Sezione INFN di Roma Tor Vergata, Roma, Italy*

[26] *Sezione INFN di Roma La Sapienza, Roma, Italy*

[27] *Henryk Niewodniczanski Institute of Nuclear Physics Polish Academy of Sciences, Kraków, Poland*

[28] *AGH — University of Science and Technology, Faculty of Physics and Applied Computer Science, Kraków, Poland*

[29] *National Center for Nuclear Research (NCBJ), Warsaw, Poland*

[30] *Horia Hulubei National Institute of Physics and Nuclear Engineering, Bucharest-Magurele, Romania*

[31] *Petersburg Nuclear Physics Institute (PNPI), Gatchina, Russia*

[32] *Institute of Theoretical and Experimental Physics (ITEP), Moscow, Russia*

[33] *Institute of Nuclear Physics, Moscow State University (SINP MSU), Moscow, Russia*

[34] *Institute for Nuclear Research of the Russian Academy of Sciences (INR RAN), Moscow, Russia*

[35] *Yandex School of Data Analysis, Moscow, Russia*

[36] *Budker Institute of Nuclear Physics (SB RAS), Novosibirsk, Russia*

[37] *Institute for High Energy Physics (IHEP), Protvino, Russia*

[38] *ICCUB, Universitat de Barcelona, Barcelona, Spain*

[39] *Universidad de Santiago de Compostela, Santiago de Compostela, Spain*

[40] *European Organization for Nuclear Research (CERN), Geneva, Switzerland*

[41] *Ecole Polytechnique Fédérale de Lausanne (EPFL), Lausanne, Switzerland*

[42] *Physik-Institut, Universität Zürich, Zürich, Switzerland*

[43] *Nikhef National Institute for Subatomic Physics, Amsterdam, The Netherlands*

[44] *Nikhef National Institute for Subatomic Physics and VU University Amsterdam, Amsterdam, The Netherlands*

[45] *NSC Kharkiv Institute of Physics and Technology (NSC KIPT), Kharkiv, Ukraine*

[46] *Institute for Nuclear Research of the National Academy of Sciences (KINR), Kyiv, Ukraine*

[47] *University of Birmingham, Birmingham, United Kingdom*

[48] *H.H. Wills Physics Laboratory, University of Bristol, Bristol, United Kingdom*

[49] *Cavendish Laboratory, University of Cambridge, Cambridge, United Kingdom*

[50] *Department of Physics, University of Warwick, Coventry, United Kingdom*

[51] *STFC Rutherford Appleton Laboratory, Didcot, United Kingdom*

[52] *School of Physics and Astronomy, University of Edinburgh, Edinburgh, United Kingdom*

[53] *School of Physics and Astronomy, University of Glasgow, Glasgow, United Kingdom*

[54] *Oliver Lodge Laboratory, University of Liverpool, Liverpool, United Kingdom*

[55] *Imperial College London, London, United Kingdom*

[56] *School of Physics and Astronomy, University of Manchester, Manchester, United Kingdom*

[57] *Department of Physics, University of Oxford, Oxford, United Kingdom*

[58] *Massachusetts Institute of Technology, Cambridge, MA, United States*

[59] *University of Cincinnati, Cincinnati, OH, United States*

[60] *University of Maryland, College Park, MD, United States*

[61] *Syracuse University, Syracuse, NY, United States*

[62] *Pontifícia Universidade Católica do Rio de Janeiro (PUC-Rio), Rio de Janeiro, Brazil, associated to[2]*

[63] *University of Chinese Academy of Sciences, Beijing, China, associated to[3]*

[64] *School of Physics and Technology, Wuhan University, Wuhan, China, associated to[3]*

[65] *Institute of Particle Physics, Central China Normal University, Wuhan, Hubei, China, associated to[3]*

[66] *Departamento de Fisica , Universidad Nacional de Colombia, Bogota, Colombia, associated to[8]*

[67] *Institut für Physik, Universität Rostock, Rostock, Germany, associated to[12]*

[68] *National Research Centre Kurchatov Institute, Moscow, Russia, associated to[32]*

[69] *Instituto de Fisica Corpuscular (IFIC), Universitat de Valencia-CSIC, Valencia, Spain, associated to[38]*

[70] *Van Swinderen Institute, University of Groningen, Groningen, The Netherlands, associated to[43]*

[a] *Universidade Federal do Triângulo Mineiro (UFTM), Uberaba-MG, Brazil*

[b] *Laboratoire Leprince-Ringuet, Palaiseau, France*

[c] *P.N. Lebedev Physical Institute, Russian Academy of Science (LPI RAS), Moscow, Russia*

[d] *Università di Bari, Bari, Italy*

[e] *Università di Bologna, Bologna, Italy*

[f] *Università di Cagliari, Cagliari, Italy*

[g] *Università di Ferrara, Ferrara, Italy*

[h] *Università di Genova, Genova, Italy*

[i] *Università di Milano Bicocca, Milano, Italy*

[j] *Università di Roma Tor Vergata, Roma, Italy*

[k] *Università di Roma La Sapienza, Roma, Italy*

[l] *AGH - University of Science and Technology, Faculty of Computer Science, Electronics and Telecommunications, Kraków, Poland*

[m] *LIFAELS, La Salle, Universitat Ramon Llull, Barcelona, Spain*

[n] *Hanoi University of Science, Hanoi, Viet Nam*

[o] *Università di Padova, Padova, Italy*

[p] *Università di Pisa, Pisa, Italy*

[q] *Università degli Studi di Milano, Milano, Italy*

[r] *Università di Urbino, Urbino, Italy*

[s] *Università della Basilicata, Potenza, Italy*

[t] *Scuola Normale Superiore, Pisa, Italy*

[u] *Università di Modena e Reggio Emilia, Modena, Italy*

[v] *Iligan Institute of Technology (IIT), Iligan, Philippines*

[w] *Novosibirsk State University, Novosibirsk, Russia*

[†] *Deceased*